

Quantum unary approach to option pricing

Sergi Ramos-Calderer,¹ Adrián Pérez-Salinas,^{1,2} Diego García-Martín,^{1,2,3} Carlos Bravo-Prieto,^{1,2}
Jorge Cortada,⁴ Jordi Planagumà,⁴ and José I. Latorre^{1,5,6}

¹*Departament de Física Quàntica i Astrofísica and Institut de Ciències del Cosmos (ICCUB),
Universitat de Barcelona, Martí i Franquès 1, 08028 Barcelona, Spain.*

²*Barcelona Supercomputing Center (BSC), Spain.*

³*Instituto de Física Teórica, UAM-CSIC, Madrid, Spain.*

⁴*Caixabank, Barcelona, Spain.*

⁵*Center for Quantum Technologies, National University of Singapore, Singapore.*

⁶*Technology Innovation Institute, Abu Dhabi.*

(Dated: September 2019)

We present a novel quantum algorithm for European option pricing in finance, where the key idea is to work in the unary representation of the asset value. The algorithm needs novel circuitry and is divided in three parts: first, the amplitude distribution corresponding to the asset value at maturity is generated using a low depth circuit; second, the computation of the expected return is computed with simple controlled gates; and third, standard amplitude amplification is used to gain quantum advantage. Unary representation offers several advantages over the usual binary representation of asset values, and one disadvantage. On the positive side, unary representation remarkably simplifies the structure and depth of the quantum circuit. Amplitude distributions use quantum superposition to bypass the role of the classical Monte Carlo simulation. The unary representation also provides a post-selection consistency check that allows for a substantial mitigation in the error of the computation. On the negative side, unary representation offers lower resolution given a fixed number of qubits, as compared to binary algorithms. We compare the performance of both unary vs. binary option pricing algorithms using error maps, and find that unary representation may bring a relevant advantage in practise.

I. INTRODUCTION

Quantum computing provides new strategies to address problems that nowadays are considered difficult to solve by classical means. The first quantum algorithms showing a theoretical advantage of quantum computing are well-known since the 1990s, such as integer factorization to prime numbers [1] or a more efficient unstructured database search [2]. Nevertheless, current quantum devices are yet not powerful enough to run quantum algorithms that are able to compete against state-of-the-art classical algorithms. Indeed, available quantum computers are in their Noisy Intermediate-Scale Quantum (NISQ) stage [3], as errors due to decoherence, noisy gate application or read-out limit the performance of these new machines. These NISQ devices may be useful tools for a variety of applications due to the introduction of hybrid variational methods. Some of the proposed applications include chemistry [4–6], simulation [7–9], solving large systems of linear equations [10–12], state diagonalization [13, 14] or quantum machine learning [15–20]. Some exact, non-variational, quantum algorithms are also well-suited for NISQ devices [21–24].

A field that is expected to be transformed by the improvement of quantum devices is quantitative finance [25–29]. In recent years, there has been a surge of new methods and algorithms dealing with financial problems using quantum resources, such as optimization problems [30–33], which are in general hard.

Notably, pricing of financial derivatives is a most prominent problem, where many of its computational obstacles are suited to be overcome via quantum computation. Financial derivatives are contracts that allow the holder to buy (*call*) or sell (*put*) some asset for an established price (*strike*) before a future point in time (*maturity date*). The payoff of an option depends on the evolution of the asset price, which follows a stochastic process. Thus, the task of estimating the price of the option is a relevant problem in financial science. A simple, yet successful model for pricing options is the Black-Scholes model [34]. This is an analytically solvable model that predicts the asset evolution at a certain time T to obey a log-normal probability distribution. Current classical algorithms rely on computationally costly Monte Carlo simulations to estimate the expected return of options.

A few quantum algorithms have been discussed to improve on classical option pricing [35–37]. It has been shown that a quantum algorithm can provide a quadratic speedup in the number of quantum circuit runs as compared to the number of classical Monte Carlo runs needed to reach a certain precision. The basic idea is to exploit quantum amplitude estimation [38–40]. Nonetheless, this can only be achieved when an efficient way of loading the probability distribution of the asset price is available. The idea of using quantum Generative Adversarial Networks (qGAN) [41, 42] to solve this issue has been analyzed [43].

In the following, we propose a novel quantum algorithm for option pricing. The key new idea is to construct a quantum circuit that works in the unary basis of the asset value. Then, the evolution of the asset is computed using

an amplitude distributor module. Furthermore, the computation of the payoff greatly trivializes. A third part of the algorithm is common to previous approaches, namely it uses amplitude estimation. The unary scheme brings further advantage since it allows for a post-selection strategy that results in error mitigation. Our unary representation requires more qubits than a binary one, yet its performance is more robust and probably best suited to be run on NISQ devices. Unary representations have been considered in previous works [44–46].

We will illustrate our new algorithm focusing on a simple European option, whose payoff is only a function of the asset price at maturity date, when the contract must be executed. We will compare the performance of our unary quantum circuit with the previous binary quantum circuit proposal. The paper is organized as follows. We first introduce the standard ideas on option pricing in Sect. II. The novel unary quantum algorithm is presented and analyzed in Sect. III. We devote Sect. IV to recall the known binary approach, and we compare unary and binary quantum circuits in Sect. V.

II. CLASSICAL OPTION PRICING

The evolution of asset prices in financial markets is usually computed using a model established by F. Black and M. Scholes in Ref. [34]. This evolution is governed by two properties of the market, the interest rate and the volatility, which are incorporated into a stochastic differential equation. The equations controlling a set of assets are usually solved using Monte Carlo methods.

A. The Black-Scholes model

The Black-Scholes model for the evolution of an asset is based on the following stochastic differential equation [34]

$$dS_t = S_t r dt + S_t \sigma dW_t, \quad (1)$$

where r is the interest rate, σ is the volatility and W_t describes a Brownian process. Let us recall that a Brownian process W_t is a continuous stochastic evolution starting at $W_0 = 0$ and made of independent gaussian increments. To be specific, let $\mathcal{N}(\mu, \sigma_s)$ be a normal distribution with mean μ and standard deviation σ_s . Then, the increment related to two steps of the Brownian processes is $W_t - W_s \sim \mathcal{N}(0, t - s)$, for $t > s$.

The above differential equation can be solved analytically using Ito's lemma [47], whereby W_t is treated as an independent variable with the property that $(dW_t)^2$ is of the order of dt . Thus, the approximated derivative dS_t can be written as

$$dS_t = \left(\frac{\partial S_t}{\partial t} + \frac{1}{2} \frac{\partial^2 S_t}{\partial W_t^2} \right) dt + \frac{\partial S_t}{\partial W_t} dW_t. \quad (2)$$

By direct comparison to Eq. (1), it is straightforward to see that

$$\frac{\partial S_t}{\partial W_t} = S_t \sigma, \quad (3)$$

$$\frac{\partial S_t}{\partial t} + \frac{1}{2} \frac{\partial^2 S_t}{\partial W_t^2} = S_t r. \quad (4)$$

Using the initial condition S_0 at $t = 0$, and the Ansatz

$$S_t = S_0 \exp\{(f(t) + g(W_t))\}, \quad (5)$$

the solution for the asset price turns out to be

$$S_t = S_0 e^{(r - \frac{\sigma^2}{2})t} e^{\sigma W_t} \sim \exp\left\{\mathcal{N}\left(\left(r - \frac{\sigma^2}{2}\right)t, \sigma\sqrt{t}\right)\right\}. \quad (6)$$

This final result corresponds to a log-normal distribution.

B. European Option

An option is a derivative contract for the trading of assets. In its call/put form, the option holder can buy/sell an asset on a specific date or decline such a right. As a particular case, European options can be exercised only on a specified future date, and only depend on the actual price of the asset at that time. The price that will be paid for the asset is called *exercise price* or *strike*. The day on which the option can be exercised is called *maturity date*.

A European option payoff is defined as

$$f(S_t) = \max(0, S_T - K), \quad (7)$$

where K is the strike price and T is the maturity date. An analytical solution exists for the payoff of this kind of options.

In the following, we will propose a new quantum algorithm to price European options. Note that any quantum strategy must cope with the construction of the correct probability distribution for the asset price at maturity, and also has to be able to compute the payoff, which is a function with discontinuous derivative. Both problems have to be solved as part of the quantum circuit.

III. UNARY ALGORITHM

Let us outline a novel quantum algorithm that prices European options according to the Black-Scholes model. The main feature of the algorithm is that it works in the *unary* representation of the asset value encoded on the quantum register. That means that for every element of the basis only one qubit will be in the $|1\rangle$ state, whereas all others will remain in $|0\rangle$. A quantum register $|\psi\rangle$ made of n qubits in the unary representation can be written as

$$\begin{aligned} |\psi\rangle &= \sum_{i=0}^{n-1} \alpha_i |i\rangle \\ &= \alpha_0 |00\dots 01\rangle + \alpha_1 |00\dots 10\rangle + \dots + \alpha_{n-2} |01\dots 00\rangle + \alpha_{n-1} |10\dots 00\rangle \\ &= \sum_{i=0}^{n-1} \alpha_i \left(\bigotimes_{j=0}^{n-1} |\delta_{ij}\rangle \right), \end{aligned} \quad (8)$$

where $|i\rangle$ corresponds to the i -th element of the unary basis, δ_{ij} is the Kronecker delta and $\sum_{i=1}^n |\alpha_i|^2 = 1$. This unary representation is significantly distinct from the binary one which uses all available basis states in the Hilbert space. Previous proposals for quantum circuits that price options do use the standard binary representation [36].

Given a fixed number of qubits, the unary scheme allows for lower precision than the binary one. Indeed, only n out of 2^n basis elements of the Hilbert space are used. However, due to the natural mapping between the unary representation and the option price evolution, we will find that the probability distribution loading and the expected payoff calculation can be carried out with much simpler quantum circuits. On real devices, the potential gain of the unary representation translates into a shallower circuit depth and simpler connectivity requirements. Furthermore, the unary scheme provides means to post-select results so as to increase the faithfulness of the computation. As a matter of fact, given a precision goal, it may well turn out to be advantageous to move to the unary representation on NISQ devices, as the use of more qubits simplifies the complexity of the circuit.

The algorithm that estimates the payoff of financial derivatives is structured in three independent parts, see Fig. 2.

- (a) *Amplitude distributor*: it encodes the underlying probability distribution of an asset price into a quantum register.
- (b) *Payoff calculation*: it computes the expected payoff of the asset at maturity date. The expected payoff is encoded into the amplitude of an ancillary qubit.
- (c) *Amplitude estimation*: it speeds up the actual measurement of an outcome carrying the expected payoff.

This three-part sequence is common to unary and binary representations. In this paper we present a novel way of proceeding with the first two steps of the algorithm, that we will now discuss in further detail.

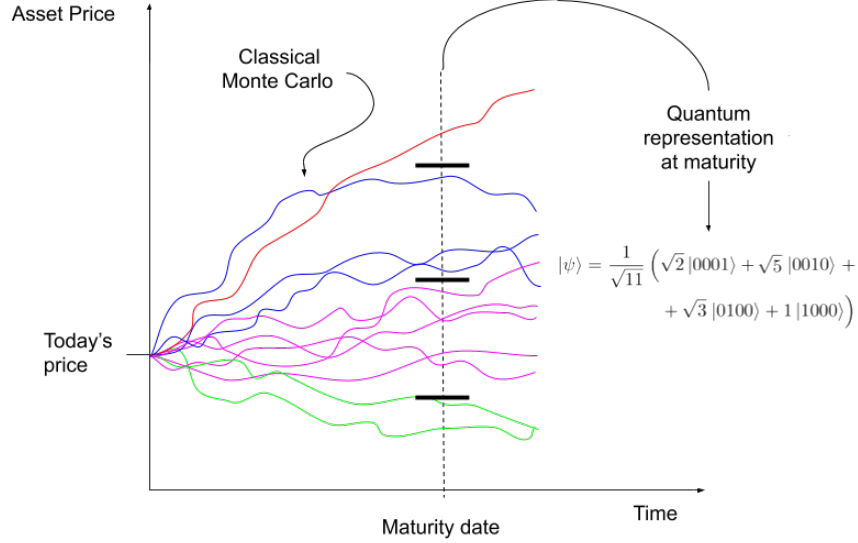


Figure 1: Scheme for the quantum representation of a given asset price at maturity date. For a given number of Monte Carlo paths, a binning scheme must be applied in such a way that the prices of the asset are separated according to its value. Each bin is mapped then to an element of the unary basis, whose coefficient is the number of Monte Carlo paths in this bin. The quantum representation of the asset price at maturity contains all possible Monte Carlo paths simultaneously. The precision is then bounded by the numbers of bins we can store on a quantum state, *i.e.* how many qubits are available.

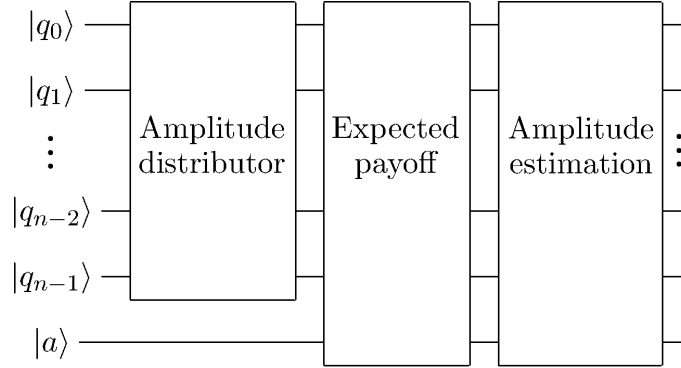


Figure 2: Basic structure of the option pricing algorithm on a quantum computer with n qubits for the register plus one ancilla to compute the expected payoff. Further amplitude estimation can be performed using different schemes that may need a different number of extra ancillary qubits. The algorithm is separated in three distinct parts, each serving a specific purpose as discussed in the main text. The components that we tackle in this paper are the first two.

A. Amplitude distributor

The probability distribution predicted by the Black-Scholes model is based on the solution of the stochastic differential equation in Sec. II A. For a given number of qubits, that is of precision, the asset price at any time can be mapped to a fixed depth circuit that distributes probabilities according to the final desired result.

The unary representation is akin to the value of the asset. In other words, for every element in the superposition describing the quantum register, the qubit which is flipped into $|1\rangle$ determines the value of the asset. The superposition of the unary basis elements accounts for the Monte Carlo spread of asset values, with their corresponding probability.

The quantum circuit generating the final register operates as a distributor of probability amplitudes. We initialize the circuit at $|0\rangle^{\otimes n}$ and then act with a Pauli X-gate on the middle qubit. At this point, the register displays a single qubit in $|1\rangle$, which is an element of the unary basis. Then, the coefficients of the register in the next step of the circuit are generated using partial-SWAP gates (also called parametrized-SWAP or SWAP power gate) between the middle qubit and its neighbors. This provides the first step to distribute the probability amplitude from the middle qubit to the rest. The procedure is repeated until the edge of the system is reached, as illustrated in Fig. 3. Specific angles can be fed into each partial-SWAP gate to obtain the target probability distribution in the unary representation.

Let us note that any final probability distribution at time t can be obtained with this circuit whose depth is independent of time, since all the necessary information is carried in the angles of the partial-SWAP gates. To be precise, given n qubits, the circuit will always be of depth $\lfloor n/2 \rfloor + 1$. The time dependency of the solution is encoded in the angles determining the partial-SWAP gates. This idea is reminiscent of the quantum circuits that describe the exact solution of the Ising model [21, 48, 49].

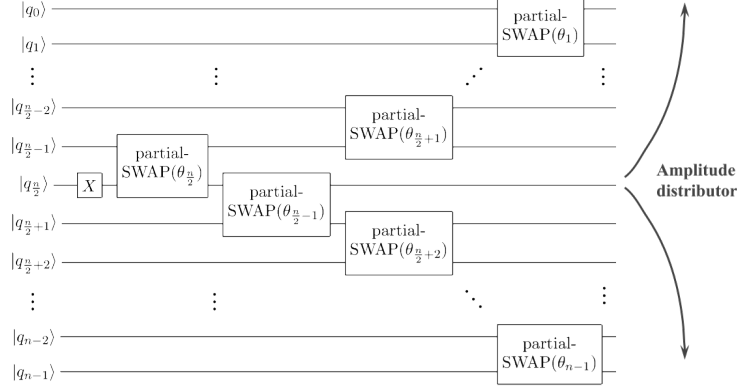


Figure 3: Quantum circuit for loading any probability distribution in the unary representation. The circuit works as a distributor of amplitude probabilities from its middle qubit to ones in the edges, using partial-SWAP gates that act only on nearest neighbors. Time dependence is encoded in the angles determining the gates.

The mapping of a probability distribution function to the unary system is dependant on $(n - 1)$ angles that need to be introduced in the partial-SWAP gates. There are two distinct situations depending on whether the final distribution probability is known exactly or not. The first case can be addressed solving an exact set of equations as described in the following. In case only the differential equation is known, but not its solution, other methods should be employed [50].

For a known probability distribution, it is possible to determine in an exact way the circuit that delivers the final register amplitudes by solving a system of n equations to solve for $n - 1$ parameters. Let us consider Fig. 3. In the unary basis, every qubit represents the basis element in which the qubit is $|1\rangle$. Thus, the coefficient of every element depends as many angles as partial-SWAP gates are needed for reaching its corresponding qubit. Thus, the central qubits of the circuit will depend only on 2 angles, and the number of dependencies increases one by one as we move to the outer part of the circuit. The very last two qubits depend on the same angles. As we move away from the middle, each qubit inherits the same angle dependency than the previous ones plus an additional rotation. Starting from the two edges, their coefficients verify the following ratios

$$\left| \frac{\alpha_0}{\alpha_1} \right|^2 = \tan^2(\theta_1/2) \quad (9)$$

$$\left| \frac{\alpha_{n-1}}{\alpha_{n-2}} \right|^2 = \tan^2(\theta_{n-1}/2). \quad (10)$$

Then we identify $|\alpha_i|^2 = p_i$, where $\{p_i\}$ is the target probability distribution. The next step corresponds to considering the qubits 1 and 2, as well as $n - 3$, $n - 2$. The relations for their coefficients must obey

$$\left| \frac{\alpha_1}{\alpha_2} \right|^2 = \cos^2(\theta_1/2) \tan^2(\theta_2/2) \quad (11)$$

$$\left| \frac{\alpha_{n-2}}{\alpha_{n-3}} \right|^2 = \cos^2(\theta_{n-1}/2) \tan^2(\theta_{n-2}/2). \quad (12)$$

Then, it is straightforward to back-substitute parameters step by step until we arrive to the central qubits. This procedure fixes completely the modulus of all coefficients.

Once the exact solution for the angles is inserted into the circuit depicted in Fig. 3, the amplitude distributor algorithm is completed. The quantum register then reads

$$|\Psi\rangle = \sum_{i=0}^{n-1} \sqrt{p_i} |i\rangle. \quad (13)$$

Note that describing a probability distribution with squared amplitudes of a quantum state allows for a free phase in every coefficient of the quantum circuit. For simplicity, we will set to zero all these relative phases by only operating with real partial-SWAP gates.

Let us turn our attention to the gates which are needed in the above circuit. Sharing probability between neighbor qubits can be achieved by introducing a two-qubit gate based on the SWAP and R_y operations. This variant on the SWAP gate performs a partial SWAP operation, where only a piece of the amplitude is transferred from one qubit to another. This operation preserves unarity, that is the state remains as a superposition of elements of the unary basis. This partial-SWAP, can be decomposed using CNOT as the basic entangling gate as

$$\text{partial-SWAP}(\theta) = \begin{pmatrix} 1 & 0 & 0 & 0 \\ 0 & \cos \theta/2 & \sin \theta/2 & 0 \\ 0 & -\sin \theta/2 & \cos \theta/2 & 0 \\ 0 & 0 & 0 & 1 \end{pmatrix} = \begin{array}{c} \text{---} \oplus \text{---} \\ | \\ \text{---} \bullet \text{---} \\ | \\ \text{---} \oplus \text{---} \\ | \\ \text{---} \bullet \text{---} \\ | \\ \text{---} \oplus \text{---} \end{array} \begin{array}{c} \text{---} \oplus \text{---} \\ | \\ \text{---} \bullet \text{---} \\ | \\ \text{---} \oplus \text{---} \\ | \\ \text{---} \bullet \text{---} \\ | \\ \text{---} \oplus \text{---} \end{array} R_y(\theta) \begin{array}{c} \text{---} \oplus \text{---} \\ | \\ \text{---} \bullet \text{---} \\ | \\ \text{---} \oplus \text{---} \\ | \\ \text{---} \bullet \text{---} \\ | \\ \text{---} \oplus \text{---} \end{array}, \quad (14)$$

where the usual CNOT gate in the center of the conventional SWAP gate has been substituted by a cR_y gate. In turn, the cR_y operation can be reworked as a combination of single-qubit gates and CNOT gates [51]:

$$\begin{array}{c} \text{---} \bullet \text{---} \\ | \\ \text{---} R_y(\theta) \text{---} \end{array} = \begin{array}{c} \text{---} \bullet \text{---} \\ | \\ \text{---} R_y(\theta/2) \oplus R_y(-\theta/2) \text{---} \\ | \\ \text{---} \bullet \text{---} \end{array}. \quad (15)$$

This decomposition will come into play for the expected payoff calculation algorithm as well.

Moreover, the partial-SWAP gate may be substituted with a partial-iSWAP gate which performs the same purpose of amplitude sharing. This partial-iSWAP gate,

$$\text{partial-iSWAP} = \begin{pmatrix} 1 & 0 & 0 & 0 \\ 0 & \cos \theta/2 & -i \sin \theta/2 & 0 \\ 0 & i \sin \theta/2 & \cos \theta/2 & 0 \\ 0 & 0 & 0 & 1 \end{pmatrix}, \quad (16)$$

is a universal entangling gate that comes naturally from the capacitive coupling of superconducting qubits [52, 53]. For the purposes of this algorithm, both the CNOT and partial-iSWAP basis gates are analogous, but the direct modeling to partial-iSWAPs can economize the total number of required gates for the amplitude distributor. Partial-iSWAP gates can be used to decompose CNOT gates. More explicitly, a CNOT gate can be reproduced with two iSWAP gates, and 5 single qubit gates.

B. Expected payoff calculation

The expected payoff calculation circuit builds upon the action of the amplitude distributor to encode the expected return on an ancillary qubit. The unary representation allows for a simple algorithm to accomplish this task. The procedure will prepare an entangled state in the form

$$|\Psi\rangle = \sqrt{1 - A^2} |\psi_0\rangle |0\rangle + A |\psi_1\rangle |1\rangle, \quad (17)$$

where $|\psi_{0,1}\rangle$ are states keeping in their superpositions the basis elements below and above the strike, respectively. The payoff is encoded within the amplitude A , with $|A|^2 \leq 1$, ready for amplitude estimation [40].

The relevant point to encode the payoff of an European option in an ancillary qubit is to distinguish in the quantum register whether the option price S_i is above or below the strike K . This task turns out to be very simple when working in the unary representation, as opposed to the binary one where a comparator needs to be introduced. To be explicit, the computation of the payoff can be achieved by applying cR_y rotations controlled by the qubits that encode a price higher than the accorded strike K . These cR_y gates will only span over those qubits that represent asset values larger than the strike. Note that the depth of the circuit will be $n - k$, where k is the unary label of the strike K , see Fig. 4.

The rotation angle for each cR_y depends on the contribution of the qubit to the expected payoff. This can be achieved using

$$\phi_i = 2 \arcsin \sqrt{\frac{S_i - K}{S_{\max} - K}}, \quad (18)$$

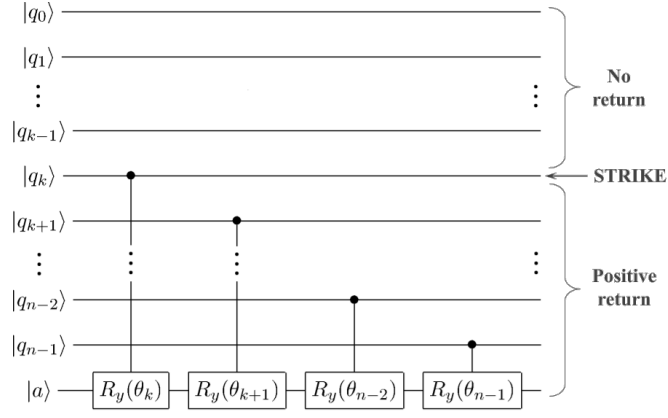


Figure 4: Quantum circuit that encodes the expected payoff in an ancillary qubit in the unary representation. Each qubit with a mapped option price higher than the designated strike controls a cR_y gate on the ancilla, where the rotation angle is a function of its contribution to the expected payoff.

where the denominator inside the arcsin argument is introduced for normalization.

Once the angles are plugged in their respective gates, the resulting state of the quantum system is

$$|\Psi\rangle = \sum_{S_i \leq K}^{n-1} \sqrt{p_i} |i\rangle |0\rangle + \sum_{S_i > K}^{n-1} \sqrt{p_i} \cos(\phi_i/2) |i\rangle |0\rangle + \sum_{S_i > K}^{n-1} \sqrt{p_i} \sqrt{\frac{S_i - K}{S_{max} - K}} |i\rangle |1\rangle. \quad (19)$$

The state is now in the form of Eq. (17). It is straightforward to see that the probability of measuring $|1\rangle$ in the ancillary qubit is

$$P(|1\rangle) = \sum_{S_i > K} p_i \frac{S_i - K}{S_{max} - K}. \quad (20)$$

In order to recover the encoded expected payoff, we need to measure the probability of obtaining $|1\rangle$ for the ancilla and then multiply it by the normalization factor $S_{max} - K$. Note that the form of the state is such that further amplitude estimation can be performed.

C. Full circuit

Once the probability loading and expected payoff calculation are combined, the unary algorithm we propose is complete. The full circuit is showcased in Fig. 5 using an example with 7 qubits plus an ancilla.

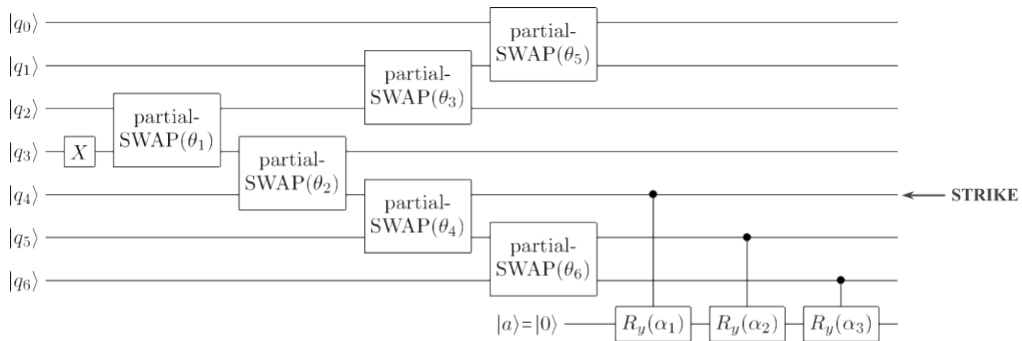


Figure 5: Total circuit for the pricing of European derivatives in the unary representation for $n = 7$ qubits. The strike price K corresponds to qubit q_4 in this example.

The number of gates the algorithm requires scales linearly with the number of qubits, that is $\mathcal{O}(n)$. This scaling corresponds to a linear scaling with the precision in the discretization of the probability distribution.

D. Ideal chip architecture

The structure of the unary algorithm allows for a simple chip design. In order to upload the desired probability distribution to the quantum register only local interactions between first neighbor qubits are required. Therefore, qubits can be arranged on a single line with two-local interactions. Such a connectivity is perfectly suited to carry out the algorithm. In order to compute the expected payoff, the ancillary qubit needs to interact with the rest of the quantum register. This structure is outlined in Fig. 6 for an arbitrary number of qubits.

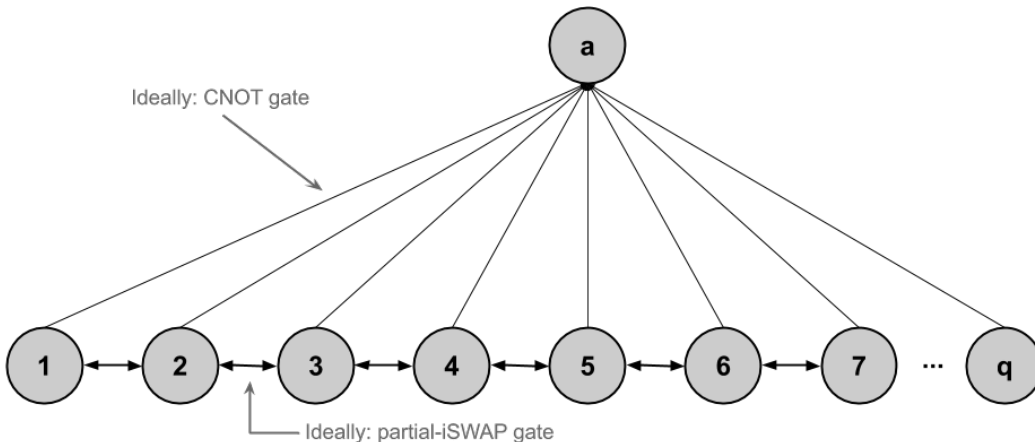


Figure 6: Ideal chip architecture to implement the unary algorithm for option pricing. Only a single ancilla qubit has to be non-locally controlled by the rest of the qubits. All other interactions are first nearest neighbor gates. This design scales linearly with the number of qubits.

The simplicity of the architecture needed to implement the unary algorithm might yield an advantage over alternative algorithms in NISQ computers. Note also that superconducting qubits allow for a natural implementation of the partial-iSWAP gate [52]. This realization of the quantum circuit would result in a decrease of the number of needed gates by factor of 6 in the amplitude distributor module.

E. Gate count

The unary algorithm needs $\mathcal{O}(n)$ partial-SWAP gates in order to distribute the amplitude and $\mathcal{O}(\alpha n)$ controlled- R_y gates to encode the payoff in an ancillary qubit, where $0 \leq \alpha \leq 1$ depends on the strike price K . However, actual quantum devices operate using a native set of gates that serve to construct any other unitary. We present in Table I the gate count of the total circuit as a function of the number of qubits, using either CNOT or partial-iSWAP as the native entangling gate. The gate count assumes the simple ideal chip structure, see Fig. 6, that requires first neighbor interactions and an ancilla connected to the rest of the qubits.

The partial-iSWAP gate introduces a substantial gain for the amplitude distributor but requires more gates in order to implement the payoff calculation. If both partial-iSWAP interaction between nearest neighbors and CNOT-based connection with the single ancilla are implemented, the best scaling of the total algorithm would be achieved. To be precise, the total number of gates would be $(4\alpha + 1)n + 1$, and the depth of the circuit would become $(4\alpha + \frac{1}{2})n$.

F. Error mitigation

NISQ era algorithms need to be resilient against gate errors and decoherence, since fault-tolerant logical qubits are still far from being a reality. The unary representation we are proposing here to deal with option pricing turns out to offer a post-selection strategy that manages to mitigate different type of errors.

The key idea behind the possibility of accomplishing error mitigation is that unary algorithms should ideally work within a subspace of the Hilbert space, namely all terms superposed in the quantum register must contain a single qubit in the $|1\rangle$ state, excluding the ancilla. As a consequence, the read-out of any measurement should reflect this

	CNOT		partial-iSWAP	
	Amplitude distributor	Payoff estimator	Amplitude distributor	Payoff estimator
1-qubit gates	$2n$	$2\alpha n$	1	$\alpha 10n$
2-qubit gates	$4n$	$2\alpha n$	n	$\alpha 5n$
Circuit depth	$3n$	$4\alpha n$	$n/2$	$15\alpha n$

Table I: Scaling of the number of 1- and 2-qubit gates and circuit depth as a function of the number of qubits n representing asset value, for the amplitude distributor and payoff estimator. In case the experimental device can implement both CNOT and partial-iSWAP, the total amount of gates and total depth would be reduced. The parameter $0 \leq \alpha \leq 1$ depends on the position of the strike in the qubit register.

fact. It is then possible to reject any outcome that does not fulfil this requirement. As a matter of fact, a number of repetitions of the experiment must be discarded, what results in a reduction of errors.

We will investigate in detail the performance of unary vs. binary circuits for option pricing in Sec. V. There we will find out that the unary representation is advantageous to the binary one, when targeting the same realistic precision.

IV. BINARY ALGORITHM

For the sake of completeness, we now present a binary algorithm for option pricing, as introduced in Ref. [35]. We will be comparing both unary and binary approaches in Sec. V.

The binary algorithm is also divided in three parts, as the unary one, namely (a) amplitude distribution loading, (b) expected payoff computation and (c) amplitude estimation. The main difference is that all computational-basis states are used to codify the discretized probability distribution of an asset price at maturity time. This implies steps (a) and (b) will require completely different quantum circuitry. We now proceed to describe these first two steps for the binary case.

A. Amplitude distribution loading

Uploading probability distributions onto quantum states is a very general problem that was considered in [54]. In this work, it was claimed that any probability distribution that is efficiently integrable on a classical computer, *e.g.* log-concave distributions, can be loaded efficiently onto a quantum state. However, several authors [55, 56] have pointed out that the method proposed there requires pre-calculating a number of integrals that grows exponentially with the number of qubits. In the case of option pricing, a reasonable precision requires a moderate number of qubits in the unary representation and many less in the binary representation. But, as a matter of fact, the reduction to a logarithmic number of qubits in the binary representation is compensated by the exponential effort needed to prepare the probability distribution. That is, in practise, both unary and binary representations require equal effort to pre-process the probability distribution to later encode it in the quantum register.

An alternative method to encode a probability distribution in a quantum state is the use of so-called quantum Generative Adversarial Networks (qGANs) [41–43]. In this scheme, two agents, a generator and a discriminator compete against each other. The generator learns to produce data that mimics the underlying probability distribution, trying to deceive the discriminator into believing that the new data is faithful. On the other hand, the discriminator has to learn how to tell apart the real data from the data produced by the generator. This quantum adversarial game has a unique endpoint: Nash equilibrium is reached when the generator learns to produce states that deliver probability outcomes that are indistinguishable from the desired probability distribution, and the discriminator cannot tell them apart. In order to upload probability distributions onto quantum states using qGANs, a parametrized quantum circuit may play the role of a generator, whereas the discriminator may be a classical neural network.

At present, there is still a lack of precise understanding on how to efficiently upload probability distributions on a quantum computer in binary representation, which makes rigorous complexity analysis in terms of the number of gates difficult.

B. Payoff computation

A useful feature of the unary algorithm is that, given a strike K , one can directly know which qubits will not contribute to the expected return of the option, and therefore adjust the quantum circuit. This is only possible since the unary representation maps directly to the asset price. In a binary encoded setting one needs to compute explicitly which basis elements will make a non-zero contribution to the expected payoff. Hence the need of a quantum comparator, U_K , that singles out the values of S_T that are smaller than the strike price K . This comparator requires the use of $n + 1$ ancillary qubits, one of which is retained after the computation. Its action is given by

$$|\psi\rangle|0\rangle \xrightarrow{U_K} \sum_{S_i < K} \sqrt{p_i} |e_i\rangle|0\rangle + \sum_{S_i \geq K} \sqrt{p_i} |e_i\rangle|1\rangle, \quad (21)$$

where $\{|e_i\rangle\}$ is the computational basis and $\{S_i\}$ are the asset values at maturity associated to computational-basis vectors. The quantum circuit implementing Eq. (21) can be constructed using cNOTs, Toffoli gates and OR gates, see Fig. 7. In order to understand the way this circuit works, let us consider the case where the discretization of the interval $[S_{max} - S_{min}]$ is uniform. In this case, the relation between $\{S_i\}$ and $\{|e_i\rangle\}$ is

$$S_i = S_{min} + \frac{e_i (S_{max} - S_{min})}{2^n}. \quad (22)$$

This implies that

$$S_i > K \Leftrightarrow e_i > \frac{2^n (K - S_{min})}{S_{max} - S_{min}} \equiv K'. \quad (23)$$

The idea goes as follows. First, we classically compute the two's complement of K' , *i.e.* $2^n - K'$, and store it in binary format in a classical array of n bits, $t[j]$ with $j \in [0, 1, \dots, n-1]$. Then, using n ancillas, $|a_0 \dots a_{n-1}\rangle$, initialized to $|0 \dots 0\rangle$, we compute the carry bits of the bitwise addition between t and $\{e_i\}$, and store them in superposition into $|a_0 \dots a_{n-1}\rangle$. If $e_i > K'$, then necessarily $a_{n-1} = 1$.

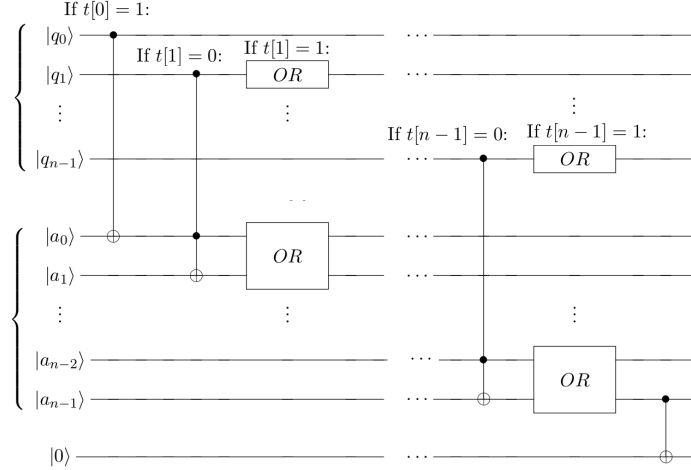


Figure 7: Quantum comparator, U_K .

The exact circuit needed for a given strike will depend upon the values of the bits in t . If $t[j] = 0$, then there will be a carry bit at position j if and only if there is a carry bit at position $j-1$ and the j -th bit of e_i is 1. This is computed with a Toffoli gate. On the other hand, if $t[j] = 1$, there will be a carry bit at position j if and only if there is a carry bit at position $j-1$ or the j -th bit of e_i is 1. This is computed with an OR gate, shown in Fig.8. Finally, there will be a carry bit at a_0 if and only if $t[0] = 1$ and the first bit of e_i is 1. This is achieved with a simple CNOT gate. As explained above, if $e_i \geq K'$, then a_{n-1} must be equal to 1. Hence, applying a CNOT gate controlled by the qubit $|a_{n-1}\rangle$ and targeted at the ancilla, the desired state in Eq. (21) is obtained.

Once U_k has been applied, the next step is to encode the expected payoff of the option into the amplitudes of a new ancilla. The final state to be created should be

$$\sum_{S_i < K} \sqrt{p_i} |e_i\rangle|0\rangle [\cos(g_0)|0\rangle + \sin(g_0)|1\rangle] + \sum_{S_i \geq K} \sqrt{p_i} |e_i\rangle|1\rangle [\cos(g_0 + g(i))|0\rangle + \sin(g_0 + g(i))|1\rangle], \quad (24)$$

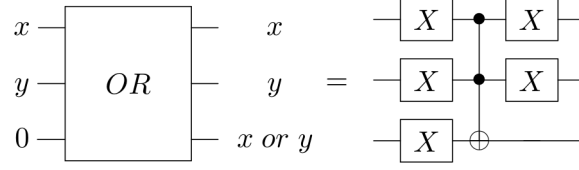


Figure 8: Decomposition of the OR gate in terms of single-qubit and Toffoli gates.

where

$$g_0 = \frac{\pi}{4} - c \quad , \quad g(i) = \frac{2c(e_i - K')}{e_{max} - K'} \quad , \quad (25)$$

with c a constant such that $c \in [0, 1]$. Thus, the probability of measuring the second ancilla in the $|1\rangle$ state in (24) is

$$\text{Prob}(1) = \sum_{S_i < K} p_i \sin^2(g_0) + \sum_{S_i \geq K} p_i \sin^2(g_0 + g(i)) \quad . \quad (26)$$

Using the approximation

$$\sin^2\left(cf(i) + \frac{\pi}{4}\right) = \frac{1}{2} + cf(i) + O(c^3 f^3(i)) \quad , \quad (27)$$

to first order, which follows from Taylor-expanding $\sin^2(f(x) + \frac{\pi}{4})$ around $f(x) = 0$, the probability becomes

$$\text{Prob}(1) \simeq \sum_{S_i < K} p_i \left(\frac{1}{2} - c\right) + \sum_{S_i \geq K} p_i \left(\frac{1}{2} + c \left[\frac{2(e_i - K')}{e_{max} - K'} - 1\right]\right) = \frac{1}{2} - c + \frac{2c}{e_{max} - K'} \sum_{S_i \geq K} p_i (e_i - K') \quad . \quad (28)$$

It is important to note that the approximation made in Eq. (28) is valid since $cf(i) = c \left[\frac{2(e_i - K')}{e_{max} - K'} - 1\right] \in [-c, c]$. Reversing the change from Eq. (23), namely

$$\sum_{S_i \geq K} p_i (S_i - K) = \frac{S_{max} - S_{min}}{2^n} \sum_{S_i \geq K} p_i (e_i - K') \quad , \quad (29)$$

the expected payoff function, *i.e.* $\sum_{S_i \geq K} p_i (S_i - K)$, can be recovered from the probability of measuring 1 in the ancilla, Eq. (28), since c, K, S_{max} are all known.

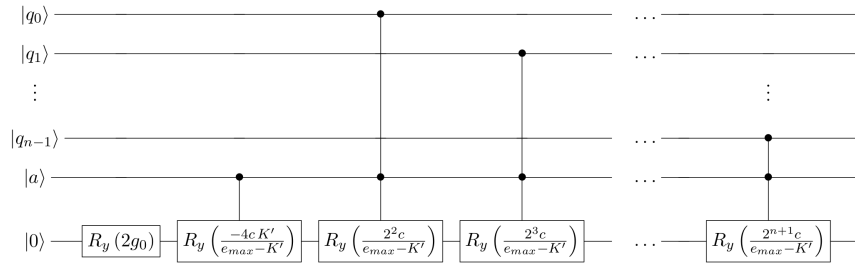


Figure 9: Encoding of the expected return of a European option into the amplitudes of an ancilla qubit in binary representation.

The quantum circuit that produces the final state (24) from (21) is composed of n ccR_y gates, plus one R_y and one cR_y gate, shown in Fig. 9. The decomposition of a ccR_y gate in terms of CNOTs and cR_y gates is shown in Fig. 10.

C. Ideal chip architecture

The binary algorithm for payoff calculation needs non-local chip connectivity. For the sake of comparison with the simplest chip architecture we presented for the unary algorithm, the most basic connectivity needed to perform the

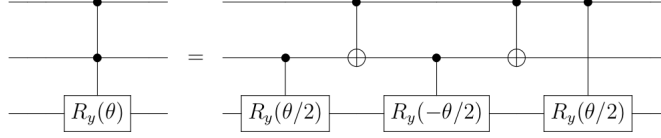


Figure 10: Decomposition of a ccR_y gate in terms of cNOTs and cR_y gates.

steps described for the binary scheme is displayed in Fig. 11. The number of necessary qubits for the binary algorithm scales better than the unary approach, despite the increasing number of ancillary qubits required. Nevertheless, the need of Toffoli gates and full connectivity will eliminate this advantage in practical problems.

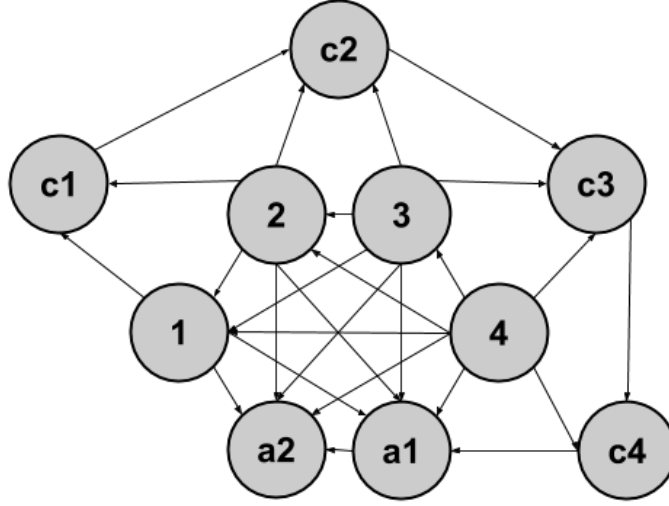


Figure 11: Ideal chip architecture to implement the binary algorithm for option pricing with 4 qubits of precision. The algorithm requires a number of ancillary qubits equal to the precision qubits plus two, 4+2 in this example. Full connectivity is still needed between the precision qubits and two ancillas.

D. Gate count

The scaling of the gate count for the binary algorithm is displayed in Table II. We compare the scaling when using CNOT or partial-iSWAP as native gates. The CNOT gate turns out to be more convenient for the binary algorithm. These results include the part of the algorithm that produces the uploading of the probability distribution into the quantum register (hence the dependence on the number of layers of the variational circuit), but it does not take into account the training required by the qGAN.

	CNOT		partial-iSWAP	
	qGAN	Payoff estimator	qGAN	Payoff estimator
1 qubit gates	$3nl$	$(16+5\alpha)n$	$8nl$	$(86+5\alpha)n$
2 qubit gates	nl	$14n$	$2nl$	$28n$
Circuit depth	$nl+1$	$(27+2\alpha)n$	$6nl+1$	$(97+2\alpha)n$

Table II: Scaling of the number of 1- and 2-qubit gates and circuit depth as a function of the number of qubits n representing the asset value in binary representation, for the amplitude distributor and payoff estimator. We compare this scaling in case CNOT or partial-iSWAP gates are implemented. Note the large overheads due to the use of Toffoli gates. The parameter $0 \leq \alpha \leq 1$ characterizes the number of 1s in the binary representation of the strike price. For the amplitude distributor, l is the number of layers a qGAN needs to successfully upload the data.

This gate count is performed assuming full connectivity, or at least the connectivity presented in Fig. 11. Existing quantum devices need to implement extra SWAP gates to account for insufficient connections, which are not taken into account in this calculations. Therefore, the gate counting on a computer with less than this ideal connectivity will result in a worse scaling.

Let us emphasize that the gate overhead for the unary representation is much lower than the one for the binary case. This is due to the fact that the unary circuit does not require any three-qubit gate. This simplification is eclipsed by the gain in precision for large n , provided that an efficient uploading of probability distributions is found for the binary case. The detailed gate count comparing unary *vs.* binary circuits is shown in Fig. 12, where we have taken $\alpha = \frac{1}{2}$, $l = \frac{\log_2 n}{2}$. In order to compare like with like, the comparison of scaling is made as follows. For a given number of n bins, which directly relate to precision, we take n qubits in the unary representation and only $\log_2 n$ in the binary one. Note that the overhead in the binary representation makes the unary one more convenient for a number of bins less than ~ 100 . In practise, the connectivity requirements further benefits the unary representation over the binary one.

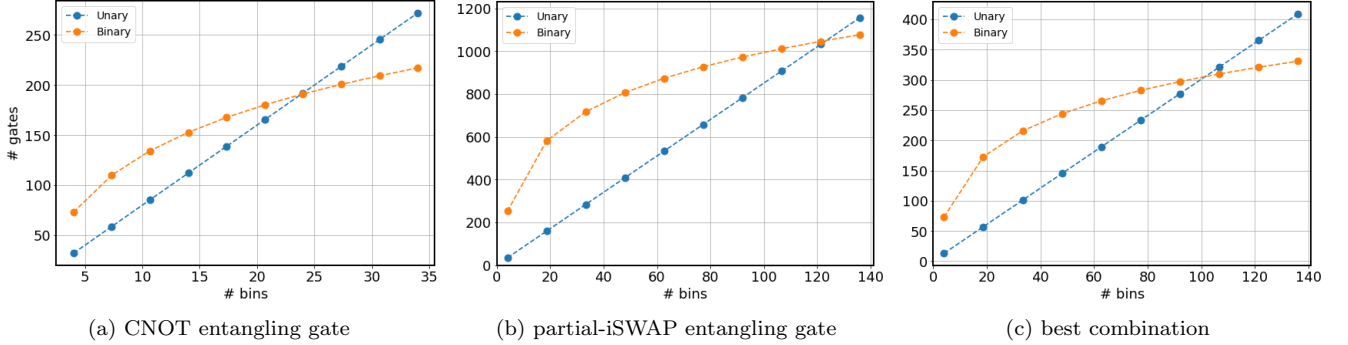


Figure 12: Scaling of the number of gates required for the total algorithm with the number of bins, as a function of different native gates: (a) CNOT gates, (b) partial-iSWAP gates and (c) the best possible combination. The scaling is calculated assuming ideal connectivity.

The unary algorithm needs, once decomposed into basic gates, less than $6n - 4$ entangling CNOT gates and less than $4n - 2$ single qubit gates, further explored in III E. This is reduced by several factors if partial-iSWAP gates are native in the quantum device, as only $n - 1$ entangling gates would be needed for the probability loading algorithm. This upper bound hinges on the position of the strike price K as it greatly reduces the amount of gates on the second step of the algorithm. This scaling confirms that this unary representation would get outperformed by the full binary space for large number of bins provided the devices performed gates with no error. However, if quantum resources are limited, as in NISQ devices, circumstances are favorable for the unary representation.

V. SIMULATIONS

The circuits we present in this paper can be simulated using the tools provided by the Python package *Qiskit* [57]. We first consider both the unary and binary algorithms in ideal conditions, that is we verify the performance of the quantum circuits in the absence of any noise. Then, we test both of them under increasing amount of different simulated noise in order to attest which of the two procedures is more advantageous for NISQ devices.

A. Amplitude distribution loading

The log-normal probability distribution used for the simulations is generated in accordance with the Black-Scholes model discussed in Sec. II. We work with an example, chosen such that the asset price at $t = 0$ is $S_0 = 2$, the volatility of the asset is $\sigma = 40\%$, the risk-free market rate is $r = 4\%$ and the maturity time is $T = 0.1$ years. The accorded strike price for the asset is set to be $K = 1.9$. The simulation of the asset price ranges up to three standard deviations from the mean value of the distribution.

The final result of loading the amplitude distribution in the quantum register is equivalent in both unary and binary representations. However, the binary algorithm requires the training of qGANs, that computationally is going to be

more costly, and potentially noisy if performed on a real quantum computer. Meanwhile, the unary algorithm requires solving a system of equations and the quantum circuit uploads it directly.

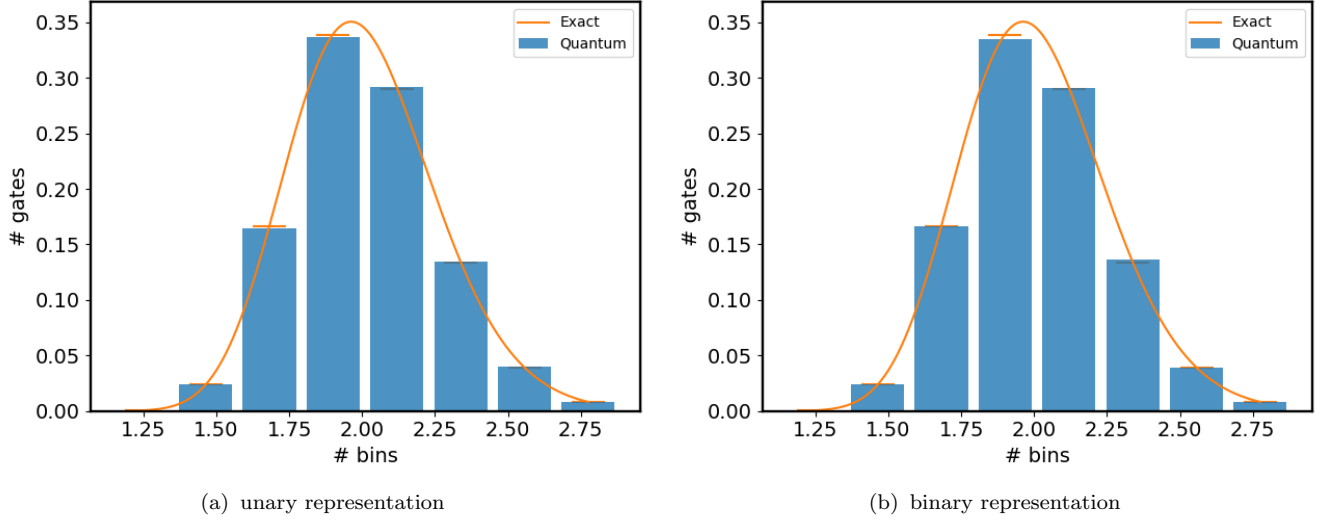


Figure 13: The probability distribution is shown for equivalent 8 qubit unary and 3 qubit binary algorithms. The orange line illustrates the classical target probability distribution. Each probability is estimated using 10^5 samples. Both algorithms reach the desired target distribution, but the unary one achieves it in a single run of the circuit while the binary relies on a variational method.

B. Expected payoff calculation

In terms of payoff calculation, the algorithms diverge slightly. Classically, with a precision of 10^4 bins, the estimated payoff for this financial option is 0.1595, that we take as exact for comparison with the quantum strategies. In order to compare like with like, on the quantum side we take 8 unary qubits and 3 binary qubits, that both correspond to 8 bins. The unary and the binary algorithms get similarly close to the approximate classical value. Averaging over 100 instances, in order to mitigate statistical sampling errors, the unary method outputs an expected payoff of 0.1552, while the binary scheme results in an expected payoff of 0.1502 (see Table III). Due to the complexity of the binary algorithm, errors appear that are not present in the unary.

Method	Exact	Unary	Binary
Expected payoff	0.1595	0.1552	0.1502
Percentage off (%)	—	2.98	6.17

Table III: Expected payoff calculation between the unary and binary algorithms. The expected payoff is averaged over 100 instances and compared to a precise computation via classical means. The unary algorithm is twice as precise in the payoff calculation for this computation.

The error of the expected payoff improves as more precision is demanded. In turn, this precision depends on the binning and where the strike is placed inside it. Therefore, at a large enough number of bins, the results fall within a reasonable percentage of the actual value. Exceptions may occur at small binning, yet the error starts to stabilize at 16-20 bins. At 100 bins errors for the option price go well below 1%.

C. Robustness against noise

In order to assess the robustness of the unary and binary algorithms, we simulate them in the presence of an increasing amount of noise. The accuracy of the expected payoff is used to benchmark both algorithms against bitflip and phaseflip errors of increasing magnitude. Both are considered to be Pauli errors and are characterized by the

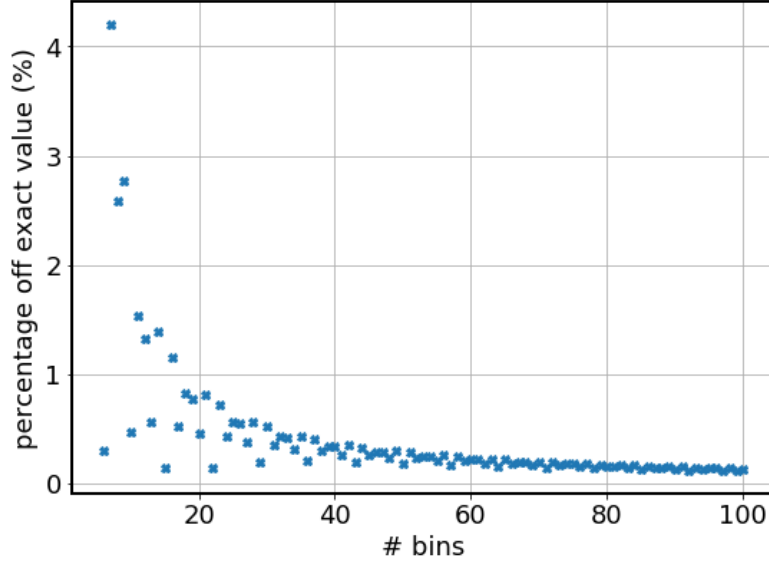


Figure 14: Percentage error from the exact value of the expected payoff for increasing number of bins in the probability distribution.

probability of occurrence of a single X or Z-gate, for bitflip and phaseflip respectively, after applying any gate in the system. In most real quantum devices, Pauli errors in two-qubit gate are more prominent than in single-qubit gates. We study errors during readout as well. Measurement errors are generally an order of magnitude higher than single-qubit Pauli errors. The simulations are performed with 8 unary and 3 binary qubits, both corresponding to 8 bins and in their respective ideal chip structures. The unary results include post-selection, which results in a clear improvement of the algorithm.

The simulations have been performed separately with the three different kinds of errors (bitflip, phaseflip, measurement). We then put them together all along the computation. The actual simulations are done using the native noise modules provided by *Qiskit*, and data are collected for increasing error probability. We show in Figs. 15(a)-15(e) the average of the relative error of the expected payoff computation when compared to the classical value. The shaded region includes 70% of the total instances used for the average. The unary algorithm, in general, has less deviation from the mean value than the binary algorithm.

The error in the expected payoff for increasing bitflip error is depicted in Fig. 15(a). This is the worst type of noise both in the unary and binary representations. Nonetheless, the unary scheme is the most robust one as it has a better scaling with the increasing error. The same amount of phaseflip error is more benign on the expected payoff computation, see Fig. 15(b). One can observe that the unary algorithm is kept below errors of 10% whereas the equivalent binary algorithm reaches over 25% of disagreement with the classical value. The unary algorithm is also more robust when faced with dephasing errors. The decrease in error that can be seen in the figures for small noise can be attributed to deviations from the ideal circuit in the direction of the exact classical payoff, effectively cancelling the inherent precision loss of the quantum algorithm with the random perturbation induced by noise.

One can compose both bitflip and phaseflip errors within the same probability of occurring to examine its effect on the expected payoff computation, see Fig. 15(c). As the errors are combined, the percentage off the classical value increases, but its behaviour indicates that the unary representation with post-selection is the most robust choice.

The case where post-selection does not help in error mitigation is when measurement errors occur. This is due to the fact that the post-selection strategy requires measuring all qubits in the system, whereas in the binary case only measurements on the ancilla qubit are needed. In Fig. 15(d) it can be seen that when the error in the readout increases past 2%, the error in the unary payoff calculation increases past the one for the binary representation. However, below a certain threshold there is still a gain in precision for the unary representation. This is not enough to overcome the gain achieved for the bitphaseflip errors as can be seen in Fig. 15(e). For increasing general errors the unary representation after post-selection remains the most robust method for payoff calculation. After the post-selection procedure is applied, at an error rate of 0.3% for single qubit gates and 3% readout error, over 55% of the data can still be used in the expected payoff computation.

Let us emphasize that current experimental errors, on the tenths of 1% for single qubit gates are such that the unary representation provides a much more faithful computation of option prices.

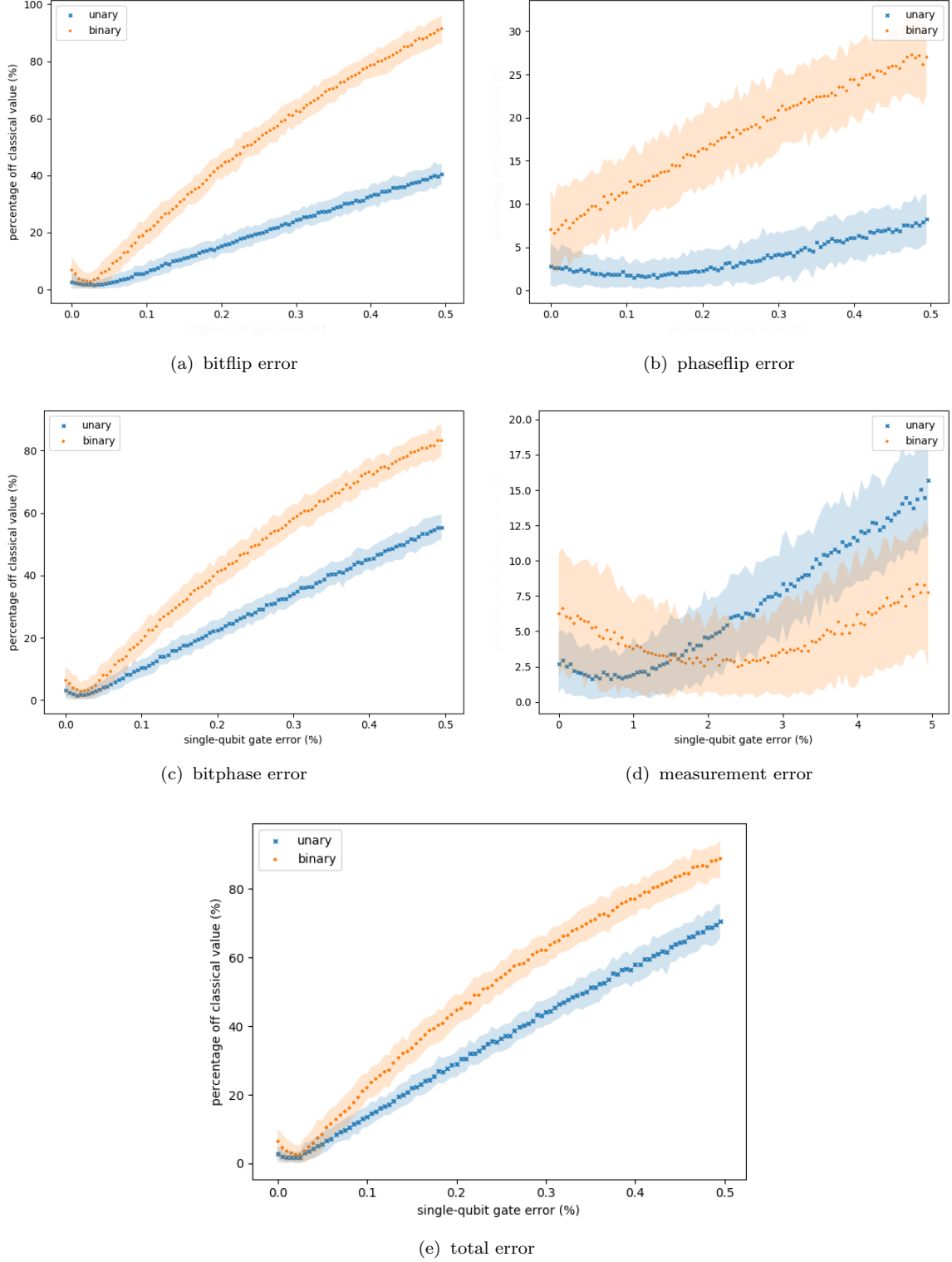


Figure 15: For equivalent 8 qubit unary and 3 qubit binary algorithms, percentage of error in the payoff calculation for increasing (a) bitflip, (b) phaseflip, (c) combination of bitflip and phaseflip, (d) measurement and (e) total error up to 0.5%, or 5% in case of measurement, for single-qubit gates, consistent with state-of-the-art devices. Two-qubit gates have twice the error. Comparison of the error of the binary algorithm with the error mitigated unary scheme averaged over 10^6 runs. The shaded region encompasses the 70% of the instances. The unary algorithm is more robust against bitflip and phaseflip errors and the combination of the two. Figure (d) showcases increased measurement noise, which affects the unary algorithm more as more qubits need to be measured. With a combination of all errors, the unary representation is the most robust algorithm for expected payoff computation.

VI. CONCLUSIONS

Finance stands as one of the fields where quantum computation may be of relevance. We have here presented a novel quantum algorithm that allows for the pricing of European options whose defining trait is that it works in the unary representation of the asset value.

We have illustrated our algorithm in the particular case of a single European option, whose maturity price for the underlying asset is obtained as the solution of a Black-Scholes equation and its expected return depends on a prefixed strike value. The global structure of our algorithm is divided in three steps: i) generation of the amplitude distribution of the asset value at maturity, ii) evaluation of the expected return given the strike value, and iii) amplitude estimation. Our algorithm needs of several new ideas to make this strategy concrete.

The very first step is to define the level of precision the algorithms should aim at. This precision is related to n , the number of qubits in the circuit. The more qubits, the more resolution we can get.

The next step corresponds to building the amplitude distribution of the asset at maturity. We have proposed to handle this problem using a circuit of depth $n/2$ that operates as a distributor of probability amplitude. this step of the algorithm substitutes the classical Monte Carlo generation of probabilities.

The computation of the expected return is particularly simple in the unary representation. It only needs a series of n conditional two-body gates from the original qubit register to an ancilla. It then follows standard amplitude amplification.

The use of unary representation seems at odds with performing precise computations. This is not so, as the precision of the expected return is an average over a sampled probability distribution which needs not have a too high resolution. We verify this statement in detail to find that less than 100 qubits are enough to have competitive computations.

Unary representation definitely offers relevant advantages over the binary one. First, it allows for a simple distribution of probability amplitudes. Second, it provides a trivial computation of expected returns. Third, unary representation should only trigger one output qubit, while reading the expected return in the ancilla. This offers a consistency check. If no output, or more than one are triggered, the run is rejected. The ability to post-select faithful runs mitigates errors and increases the performance of the quantum algorithm.

There are a number of further improvements that may be included in the algorithm. It is possible, for instance, to increase precision by taking the qubits to represent non equispaced elements in the probability distribution. It is enough to populate more densely the subtle regions of the sample distribution to gain some precision. Ideas to include multi-asset computations are also available [58].

Finally, let us mention that our unary option pricing algorithm can be implemented in quantum computers recently presented.

Acknowledgements

SRC, APS, DGM, CBP and JIL are supported by Project PJC2018-095862-B-C22. APS, DGM, CBP and JIL acknowledge CaixaBank for its support of this work through Barcelona Supercomputing Center's project CaixaBank Computación Cuántica.

-
- [1] P. W. Shor, SIAM Review **41**, 303 (1999).
 - [2] L. K. Grover, Physical Review Letters **79**, 325 (1997).
 - [3] J. Preskill, Quantum **2**, 79 (2018).
 - [4] A. Peruzzo, J. McClean, P. Shadbolt, M.-H. Yung, X.-Q. Zhou, P. J. Love, A. Aspuru-Guzik, and J. L. O'Brien, Nature Communications **5**, 4213 (2014).
 - [5] O. Higgott, D. Wang, and S. Brierley, Quantum **3**, 156 (2019).
 - [6] T. Jones, S. Endo, S. McArdle, X. Yuan, and S. C. Benjamin, Physical Review A **99**, 062304 (2019).
 - [7] Y. Li and S. C. Benjamin, Physical Review X **7**, 021050 (2017).
 - [8] C. Kokail, C. Maier, R. van Bijnen, T. Brydges, M. Joshi, P. Jurcevic, C. Muschik, P. Silvi, R. Blatt, C. Roos, *et al.*, Nature **569**, 355 (2019).
 - [9] C. Cirstoiu, Z. Holmes, J. Iosue, L. Cincio, P. J. Coles, and A. Sornborger, arXiv preprint arXiv:1910.04292 (2019).
 - [10] C. Bravo-Prieto, R. LaRose, M. Cerezo, Y. Subasi, L. Cincio, and P. J. Coles, arXiv preprint arXiv:1909.05820 (2019).
 - [11] X. Xu, J. Sun, S. Endo, Y. Li, S. C. Benjamin, and X. Yuan, arXiv preprint arXiv:1909.03898 (2019).
 - [12] H.-Y. Huang, K. Bharti, and P. Rebentrost, arXiv preprint arXiv:1909.07344 (2019).
 - [13] R. LaRose, A. Tikku, É. O'Neel-Judy, L. Cincio, and P. J. Coles, npj Quantum Information **5**, 8 (2019).
 - [14] C. Bravo-Prieto, D. García-Martín, and J. I. Latorre, arXiv preprint arXiv:1905.01353 (2019).

- [15] N. Wiebe, D. Braun, and S. Lloyd, *Physical Review Letters* **109**, 050505 (2012).
- [16] P. Rebentrost, M. Mohseni, and S. Lloyd, *Physical Review Letters* **113**, 130503 (2014).
- [17] A. Kapoor, N. Wiebe, and K. Svore, in *Advances in Neural Information Processing Systems* (2016) pp. 3999–4007.
- [18] J. Biamonte, P. Wittek, N. Pancotti, P. Rebentrost, N. Wiebe, and S. Lloyd, *Nature* **549**, 195 (2017).
- [19] Z. Zhao, A. Pozas-Kerstjens, P. Rebentrost, and P. Wittek, *Quantum Machine Intelligence* **1**, 41 (2019).
- [20] A. Pérez-Salinas, A. Cervera-Lierta, E. Gil-Fuster, and J. I. Latorre, arXiv preprint arXiv:1907.02085 (2019).
- [21] A. Cervera-Lierta, *Quantum* **2**, 114 (2018).
- [22] Y. Subasi, L. Cincio, and P. J. Coles, *Journal of Physics A: Mathematical and Theoretical* (2018).
- [23] S. Bravyi, D. Gosset, and R. Koenig, *Science* **362**, 308 (2018).
- [24] S. Bravyi, D. Gosset, R. Koenig, and M. Tomamichel, arXiv preprint arXiv:1904.01502 (2019).
- [25] R. Orús, S. Mugel, and E. Lizaso, *Reviews in Physics* , 100028 (2019).
- [26] I. Kerenidis, A. Prakash, and D. Szilágyi, in *Proceedings of the 1st ACM Conference on Advances in Financial Technologies* (ACM, 2019) pp. 147–155.
- [27] R. Orús, S. Mugel, and E. Lizaso, *Physical Review A* **99**, 060301 (2019).
- [28] A. Martín, B. Candelas, Á. Rodríguez-Rozas, J. D. Martín-Guerrero, X. Chen, L. Lamata, R. Orús, E. Solano, and M. Sanz, arXiv preprint arXiv:1904.05803 (2019).
- [29] D. J. Egger, R. G. Gutiérrez, J. C. Mestre, and S. Woerner, arXiv preprint arXiv:1907.03044 (2019).
- [30] G. Rosenberg, P. Haghnegahdar, P. Goddard, P. Carr, K. Wu, and M. López De Prado, *IEEE Journal of Selected Topics in Signal Processing* **10**, 1053 (2016).
- [31] P. Rebentrost and S. Lloyd, arXiv preprint arXiv:1811.03975 (2018).
- [32] N. Moll, P. Barkoutsos, L. S. Bishop, J. M. Chow, A. Cross, D. J. Egger, S. Filipp, A. Fuhrer, J. M. Gambetta, M. Ganzhorn, et al., *Quantum Science and Technology* **3**, 030503 (2018).
- [33] M. López de Prado, Available at SSRN 2575184 (2015).
- [34] F. Black and M. Scholes, *Journal of Political Economy* **81**, 637 (1973).
- [35] N. Stamatopoulos, D. J. Egger, Y. Sun, C. Zoufal, R. Iten, N. Shen, and S. Woerner, arXiv preprint arXiv:1905.02666 (2019).
- [36] P. Rebentrost, B. Gupta, and T. R. Bromley, *Physical Review A* **98**, 022321 (2018).
- [37] S. Woerner and D. J. Egger, *npj Quantum Information* **5**, 15 (2019).
- [38] G. Brassard, P. Hoyer, M. Mosca, and A. Tapp, *Contemporary Mathematics* **305**, 53 (2002).
- [39] S. Aaronson and P. Rall, arXiv preprint arXiv:1908.10846 (2019).
- [40] A. Montanaro, *Proceedings of the Royal Society A: Mathematical, Physical and Engineering Sciences* **471**, 20150301 (2015).
- [41] S. Lloyd and C. Weedbrook, *Physical Review Letters* **121**, 040502 (2018).
- [42] P.-L. Dallaire-Demers and N. Killoran, *Physical Review A* **98**, 012324 (2018).
- [43] C. Zoufal, A. Lucchi, and S. Woerner, arXiv preprint arXiv:1904.00043 (2019).
- [44] D. Poulin, A. Kitaev, D. S. Steiger, M. B. Hastings, and M. Troyer, *Physical review letters* **121**, 010501 (2018).
- [45] R. Babbush, C. Gidney, D. W. Berry, N. Wiebe, J. McClean, A. Paler, A. Fowler, and H. Neven, *Physical Review X* **8**, 041015 (2018).
- [46] M. Steudtner and S. Wehner, arXiv preprint arXiv:1911.00416 (2019).
- [47] K. Itô, *Proceedings of the Imperial Academy* **20**, 519 (1944).
- [48] F. Verstraete, J. I. Cirac, and J. I. Latorre, *Physical Review A* **79**, 032316 (2009).
- [49] M. Hebenstreit, D. Alsina, J. I. Latorre, and B. Kraus, *Physical Review A* **95**, 052339 (2017).
- [50] S. Iblisdir, R. Orús, and J. I. Latorre, *Physical Review B* **75**, 104305 (2007).
- [51] A. Barenco, C. H. Bennett, R. Cleve, D. P. DiVincenzo, N. Margolus, P. Shor, T. Sleator, J. A. Smolin, and H. Weinfurter, *Physical review A* **52**, 3457 (1995).
- [52] R. C. Bialczak, M. Ansmann, M. Hofheinz, E. Lucero, M. Neeley, A. O’Connell, D. Sank, H. Wang, J. Wenner, M. Steffen, et al., *Nature Physics* **6**, 409 (2010).
- [53] N. Schuch and J. Siewert, *Physical Review A* **67**, 032301 (2003).
- [54] L. Grover and T. Rudolph, arXiv preprint quant-ph/0208112 (2002).
- [55] A. Montanaro and S. Pallister, *Physical Review A* **93**, 032324 (2016).
- [56] J. J. García-Ripoll, arXiv preprint arXiv:1909.06619 (2019).
- [57] H. Abraham, I. Y. Akhalwaya, G. Aleksandrowicz, T. Alexander, G. Alexandrowics, E. Arbel, A. Asfaw, C. Azaustre, P. Barkoutsos, G. Barron, L. Bello, Y. Ben-Haim, D. Bevenius, L. S. Bishop, S. Bosch, D. Bucher, CZ, F. Cabrera, P. Calpin, L. Capelluto, J. Carballo, G. Carrascal, A. Chen, C.-F. Chen, R. Chen, J. M. Chow, C. Claus, C. Clauss, A. J. Cross, A. W. Cross, J. Cruz-Benito, Cryoris, C. Culver, A. D. Córcoles-Gonzales, S. Dague, M. Dartailh, A. R. Davila, D. Ding, E. Dumitrescu, K. Dumon, I. Duran, P. Eendebak, D. Egger, M. Everitt, P. M. Fernández, A. Frisch, A. Fuhrer, I. GOULD, J. Gacon, Gadi, B. G. Gago, J. M. Gambetta, L. Garcia, S. Garion, Gaweł-Kus, J. Gomez-Mosquera, S. de la Puente González, D. Greenberg, J. A. Gunnels, I. Haide, I. Hamamura, V. Havlicek, J. Hellmers, L. Herok, H. Horii, C. Howington, S. Hu, W. Hu, H. Imai, T. Imamichi, R. Iten, T. Itoko, A. Javadi-Abhari, Jessica, K. Johns, N. Kanazawa, A. Karazeev, P. Kassebaum, A. Kovyrshin, V. Krishnan, K. Krsulich, G. Kus, R. LaRose, R. Lambert, J. Latone, S. Lawrence, D. Liu, P. Liu, P. B. Z. Mac, Y. Maeng, A. Malyshev, J. Marecek, M. Marques, D. Mathews, A. Matsuo, D. T. McClure, C. McGarry, D. McKay, S. Meesala, A. Mezzacapo, R. Midha, Z. Mineev, M. D. Mooring, R. Morales, N. Moran, P. Murali, J. Müggenburg, D. Nadlinger, G. Nannicini, P. Nation, Y. Naveh, Nick-Singstock, P. Niroula, H. Norlen, L. J. O’Riordan, P. Ollitrault, S. Oud, D. Padilha, H. Paik, S. Perriello, A. Phan, M. Pistoia,

A. Pozas-Kerstjens, V. Prutyaynov, J. Pérez, Quintiii, R. Raymond, R. M.-C. Redondo, M. Reuter, D. M. Rodríguez, M. Ryu, M. Sandberg, N. Sathaye, B. Schmitt, C. Schnabel, T. L. Scholten, E. Schoute, I. F. Sertage, N. Shammah, Y. Shi, A. Silva, Y. Siraichi, S. Sivaram, J. A. Smolin, M. Soeken, D. Steenken, M. Stypulkoski, H. Takahashi, C. Taylor, P. Taylour, S. Thomas, M. Tillet, M. Tod, E. de la Torre, K. Trabing, M. Treinish, TrishaPe, W. Turner, Y. Vaknin, C. R. Valcarce, F. Varchon, D. Vogt-Lee, C. Vuillot, J. Weaver, R. Wieczorek, J. A. Wildstrom, R. Wille, E. Winston, J. J. Woehr, S. Woerner, R. Woo, C. J. Wood, R. Wood, S. Wood, J. Wootton, D. Yeralin, J. Yu, L. Zdanski, Zoufalc, anedumla, azulehner, bcamorrison, brandhsn, dennis-liu 1, drholmie, elfrocampeador, fanizzamarco, gruu, kanejess, klinvill, lerongil, ma5x, merav aharoni, mrossinek, ordmoj, strickroman, tigerjack, yang.luh, and yotamvakninibm, “Qiskit: An open-source framework for quantum computing,” (2019).

- [58] C. Bravo-Prieto, D. García-Martín, J. I. Latorre, A. Pérez-Salinas, and S. Ramos-Calderer, in preparation .